LETTER

doi:10.1038/nature13324

Mfsd2a is critical for the formation and function of the blood–brain barrier

Ayal Ben-Zvi[1], Baptiste Lacoste[1], Esther Kur[1], Benjamin J. Andreone[1], Yoav Mayshar[2], Han Yan[1] & Chenghua Gu[1]

The central nervous system (CNS) requires a tightly controlled environment free of toxins and pathogens to provide the proper chemical composition for neural function. This environment is maintained by the 'blood–brain barrier' (BBB), which is composed of blood vessels whose endothelial cells display specialized tight junctions and extremely low rates of transcellular vesicular transport (transcytosis)[1–3]. In concert with pericytes and astrocytes, this unique brain endothelial physiological barrier seals the CNS and controls substance influx and efflux[4–6]. Although BBB breakdown has recently been associated with initiation and perpetuation of various neurological disorders, an intact BBB is a major obstacle for drug delivery to the CNS[7–10]. A limited understanding of the molecular mechanisms that control BBB formation has hindered our ability to manipulate the BBB in disease and therapy. Here we identify mechanisms governing the establishment of a functional BBB. First, using a novel tracer-injection method for embryos, we demonstrate spatiotemporal developmental profiles of BBB functionality and find that the mouse BBB becomes functional at embryonic day 15.5 (E15.5). We then screen for BBB-specific genes expressed during BBB formation, and find that major facilitator super family domain containing 2a (*Mfsd2a*) is selectively expressed in BBB-containing blood vessels in the CNS. Genetic ablation of *Mfsd2a* results in a leaky BBB from embryonic stages through to adulthood, but the normal patterning of vascular networks is maintained. Electron microscopy examination reveals a dramatic increase in CNS-endothelial-cell vesicular transcytosis in *Mfsd2a*$^{-/-}$ mice, without obvious tight-junction defects. Finally we show that Mfsd2a endothelial expression is regulated by pericytes to facilitate BBB integrity. These findings identify Mfsd2a as a key regulator of BBB function that may act by suppressing transcytosis in CNS endothelial cells. Furthermore, our findings may aid in efforts to develop therapeutic approaches for CNS drug delivery.

Two unique features of the CNS endothelium determine BBB integrity (Extended Data Fig. 1)[2]. One is specialized tight junctions between a single endothelial cell layer lining the CNS capillaries, which form the physical seal between the blood and brain parenchyma[2]. In addition, CNS endothelial cells have lower rates of transcytosis than endothelial cells in other organs[3]. Peripheral endothelial cells display active vesicle trafficking to deliver nutrients to peripheral tissues, whereas CNS endothelial cells express transporters to selectively traffic nutrients across the BBB[1,3,11]. However, it is not clear when and how these properties are acquired. Furthermore, the molecular mechanisms that give rise to the unique properties of the CNS endothelium have not been identified. Although recent studies revealed molecular pathways involved in the development of the embryonic BBB[12–19], disruption of some of these genes affect vascular network development, making it difficult to determine whether barrier defects are primary or secondary to a broader vascular effect.

We aimed to first identify the developmental time-point when the BBB gains functional integrity, and then use that time window to profile BBB-specific genes when the BBB is actively forming, to maximize the chance of identifying key regulators. The prevailing view has been that the embryonic and perinatal BBB are not yet functional[1]. However, previous embryonic BBB functionality studies were primarily performed by transcardiac tracer perfusion, which may dramatically affect blood pressure, cause bursting of CNS capillaries, and artificially produce leakiness phenotypes[1,20]. To circumvent these obstacles, we developed a method to assess BBB integrity during mouse development, in which a small volume of tracer is injected into embryonic liver to minimize changes in blood pressure (Fig. 1a, see Supplementary Information for the method).

Using this method, we identified the timing of BBB formation in the developing mouse brain and observed a spatial and temporal pattern of 'functional-barrier genesis' (Fig. 1b). We found that in E13.5 cortex a 10-kDa dextran tracer leaked out of capillaries and was taken up by non-vascular brain parenchyma cells (Fig. 1b, top panel). At E14.5, the tracer was primarily restricted to capillaries, but tracer was still detected outside vessels (Fig. 1b, middle panel). In contrast, at E15.5, the tracer was confined to vessels with no detectable signal in the surrounding brain parenchyma, similar to the mature BBB (Fig. 1b, bottom panel). The development of BBB functionality differed across brain regions (Supplementary Information and Extended Data Fig. 2). These data demonstrate that following vessel ingression into the neural tube, the BBB gradually becomes functional as early as E15.5.

Based on the temporal profile of BBB formation, we compared expression profiles of BBB (cortex) and non-BBB (lung) endothelium at E13.5, using an Affymetrix array (Supplementary Information), and identified transcripts with significantly higher representation in cortical than lung endothelium (Fig. 2). These transcripts included transporters, transcription factors, and secreted and transmembrane proteins (Fig. 2c). We were particularly interested in transmembrane proteins, owing to their potential involvement in cell–cell interactions that regulate BBB formation.

One of the genes identified, *Mfsd2a*, had 78.8 times higher expression in cortical endothelium than in lung endothelium (Fig. 3a). *In situ* hybridization showed prominent *Mfsd2a* mRNA expression in CNS vasculature but no detectable signal in vasculature outside the CNS, such as in lung or liver (Fig. 3b). Moreover, both *Mfsd2a* mRNA and Mfsd2a protein were absent in the choroid plexus vasculature, which is part of the CNS but does not possess a BBB[1] (Fig. 3c, d, g). *Mfsd2a* expression in CNS vasculature was observed at embryonic stages (E15.5), postnatal days 2 and 5 (P2 and P5) and in adults (P90) (Fig. 3b–e and Extended Data Fig. 3). Finally, Mfsd2a protein, which is absent in the *Mfsd2a*$^{-/-}$ mice (Fig. 3e)[21], was specifically expressed in claudin-5-positive CNS endothelial cells but not in neighbouring parenchyma cells (neurons or glia) or adjacent Pdgfrβ-positive pericytes (Fig. 3f). Previously, Mfsd2a was reported to be a transmembrane protein expressed in the placenta and testis, which have highly restrictive barrier properties[22]. Together with our demonstration of Mfsd2a-specific expression in BBB-containing endothelial cells, this suggests that Mfsd2a may have a role in BBB formation and/or function.

To test this hypothesis, we examined BBB integrity in *Mfsd2a*$^{-/-}$ mice. Using our embryonic injection method, 10-kDa dextran was injected into *Mfsd2a*$^{-/-}$ and wild-type littermates at E15.5. As expected, dextran was confined within vessels of control embryos. In contrast, dextran

[1]Department of Neurobiology, Harvard Medical School, 220 Longwood Avenue, Boston, Massachusetts 02115, USA. [2]Department of Genetics, Harvard Medical School, 220 Longwood Avenue, Boston, Massachusetts 02115, USA.

leaked outside the vessels in *Mfsd2a*$^{-/-}$ embryonic brains and was found in the cortical parenchyma (Fig. 4a) and individual parenchyma cells (quantified as tracer-positive parenchyma cells per unit area of the developing lateral cortical plate; Fig. 4b). Furthermore, using imaging and spectrophotometric quantification methods[5], we found that the leaky phenotype persisted in early postnatal (Extended Data Fig. 4) and adult (Fig. 4c) *Mfsd2a*$^{-/-}$ mice. Because the sequence of Mfsd2a has similarities to the major facilitator superfamily of transporters, and Mfsd2a facilitates the transport of tunicamycin in cancer cell lines[23], we injected two non-carbohydrate-based tracers of different sizes to rule out the possibility that dextran leakiness is due to interactions with Mfsd2a. Sulfo-NHS-biotin (~550 Da) and horseradish peroxidase (HRP; ~44 kDa) tracers exhibited the leaky phenotype in *Mfsd2a*$^{-/-}$ mice (Extended Data Fig. 4a, b). Moreover, a larger molecular weight tracer, 70-kDa dextran, also displayed leakiness in *Mfsd2a*$^{-/-}$ mice (Extended Data Fig. 4d). In contrast to severe barrier leakage defects (Fig. 4a–c and Extended Data Fig. 4), brain vascular patterning was similar between *Mfsd2a*$^{-/-}$ mice and littermate controls. No abnormalities were identified in capillary density, capillary diameter or vascular branching (Fig. 4d and Extended Data Fig. 5a), in embryonic (E15.5), postnatal (P4), and adult (P70) brains of *Mfsd2a*$^{-/-}$ mice. Moreover, we found no abnormalities in cortical arterial distribution in adult *Mfsd2a*$^{-/-}$ mice (Extended Data Fig. 5b). Therefore, Mfsd2a is specifically required for proper formation of a functional BBB but not for CNS vascular morphogenesis *in vivo*. This result, together with the temporal difference between cortical vascular ingression (E10–E11) and cortical barrier-genesis (E13.5–E15.5), demonstrates that vascular morphogenesis and barrier genesis are distinct processes.

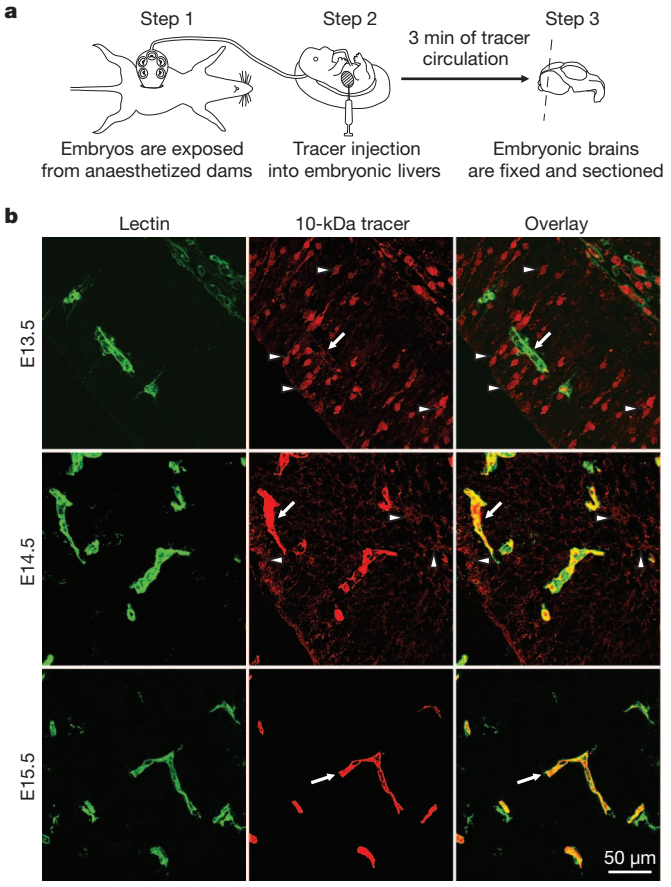

Figure 1 | A novel tracer-injection method reveals a temporal profile of functional BBB formation in the embryonic cortex. **a**, *In utero* embryonic liver tracer injection method; fenestrated liver vasculature enabled rapid tracer uptake into the embryonic circulation. **b**, Dextran-tracer injection revealed a temporal profile of functional cortical BBB formation. Representative images of dorsal cortical plates from injected embryos after capillary labelling with lectin (green, lectin; red, 10-kDa tracer). Top panel (E13.5), tracer leaked out of capillaries and was subsequently taken up by non-vascular parenchyma cells (arrowheads), with little tracer left inside capillaries (arrow). Middle panel (E14.5), tracer was primarily restricted to capillaries (arrow), with diffused tracer detectable in the parenchyma (arrowheads). Bottom panel (E15.5), tracer was confined to capillaries (arrow). $n = 6$ embryos (3 litters per age).

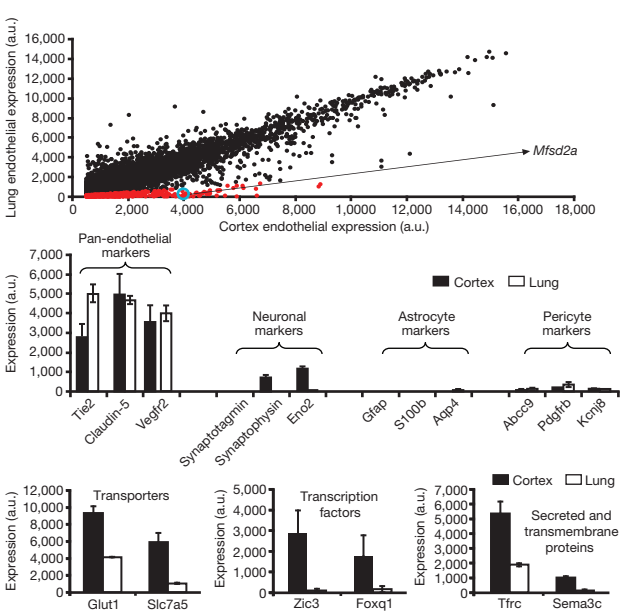

Figure 2 | Expression profiling identifies genes involved in BBB formation. **a**, Dot-plot representation of Affymetrix GeneChip data showing transcriptional profile of cortical (BBB) and lung (non-BBB) endothelial cells isolated at the critical barrier-genesis period (E13.5). Dots reflect average expression of a probe in the cortex (*x* axis) and lung (*y* axis). Cortex expression values above 500 arbitrary expression units (a.u.) are presented. Red dots indicate a fivefold higher expression in the cortex. *Mfsd2a* value is circled in blue. **b**, Pan-endothelial markers were highly represented, whereas pericyte, astrocyte, and neuronal markers were detected at extremely low levels in both cortex and lung samples. **c**, Barrier-genesis specific transporters, transcription factors, and secreted and transmembrane proteins were significantly enriched in the cortical endothelial cells. All data are mean ± s.d. $n = 4$ litters (4 biological replicates).

We next addressed whether Mfsd2a regulates endothelial tight-junction formation, transcytosis, or both. We examined these properties by electron microscopy in embryonic brains and P90 mice following intravenous HRP injection[2]. Electron microscopy failed to reveal any apparent abnormalities in the ultrastructure of endothelial tight junctions (Fig. 5a). At E17.5, tight junctions in control and *Mfsd2a*$^{-/-}$ littermates appeared normal, with electron-dense linear structures showing 'kissing points' where adjacent membranes are tightly apposed (Fig. 5a). In electron micrographs of cerebral cortex in HRP-injected adults, peroxidase activity was revealed by an electron-dense reaction product that filled the vessel lumen. In both control and *Mfsd2a*$^{-/-}$ mice, HRP penetrated the intercellular spaces between neighbouring endothelial cells only for short distances. HRP was stopped at the tight junction, creating a boundary between HRP-positive and HRP-negative regions without leakage through tight junctions (Fig. 5a). In contrast, CNS endothelium of *Mfsd2a*$^{-/-}$ mice displayed a dramatic increase in the number of vesicles, including luminal and abluminal plasma membrane-connected vesicles and free cytoplasmic vesicles, which may indicate an increased rate of transcytosis (Fig. 5b). Specifically, pinocytotic events were evidenced by type II lumen-connected vesicles pinching from the luminal plasma membrane. Greater than twofold increases in vesicle number in *Mfsd2a*$^{-/-}$ mice compared to control littermates were observed in different locations along the transcytotic pathway (Fig. 5 and Extended Data Table 2). Furthermore, the HRP reaction product in adult mice was observed in vesicles

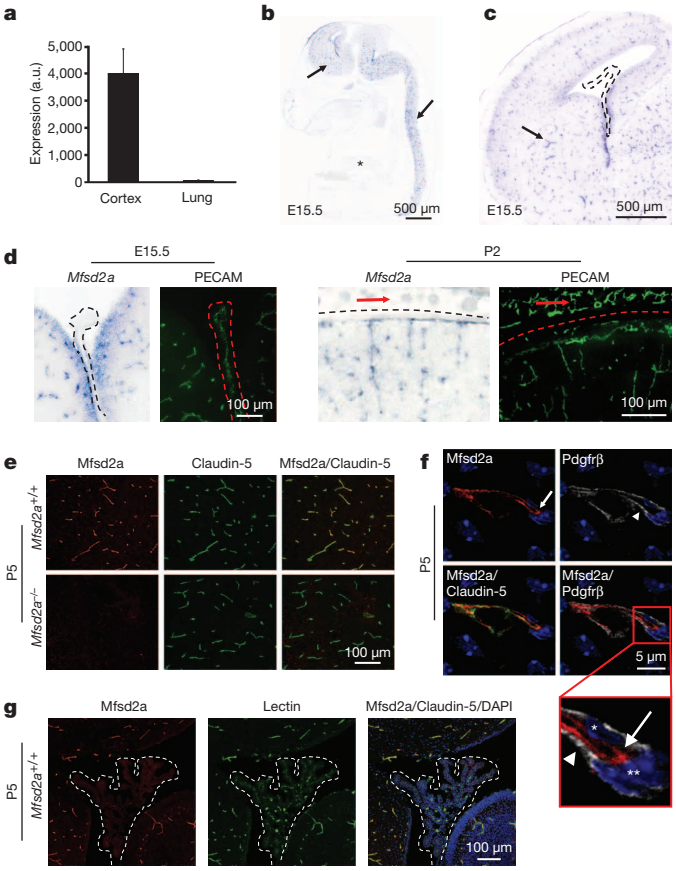

Figure 3 | *Mfsd2a* is selectively expressed in BBB-containing CNS vasculature. **a**, At E13.5, *Mfsd2a* expression in cortical endothelium was ~80-fold higher than in lung endothelium (microarray analysis, mean ± s.d.). **b–d**, Specific *Mfsd2a* expression in BBB-containing CNS vasculature (blue, *Mfsd2a in situ* hybridization; green, vessel staining (PECAM) adjacent sections). **b**, *Mfsd2a* expression at E15.5 in CNS vasculature (sagittal view of brain and spinal cord, arrows), but not in non-CNS vasculature (asterisk). **c**, *Mfsd2a* expression at E15.5 in BBB vasculature (cortex coronal view, for example, striatum, arrow), but not in non-BBB CNS vasculature (choroid plexus, dashed line). **d**, High-magnification coronal view of *Mfsd2a* expression in BBB-containing CNS vasculature but not in vasculature of the choroid plexus (left, dashed line), or outer meninges or skin (right, red arrows). **e–g**, Immunohistochemical staining of Mfsd2a protein shows specific expression in CNS endothelial cells (red, Mfsd2a; green, claudin-5 or lectin (endothelium); blue, DAPI (nuclei); grey, Pdgfrβ (pericytes)). **e**, Mfsd2a expression in the brain vasculature of wild-type mice (top panel), but not of *Mfsd2a*$^{-/-}$ mice (bottom panel). **f**, Mfsd2a expression only in claudin-5-positive endothelial cells (arrow; endothelial nucleus is indicated by an asterisk) but not in adjacent pericytes (arrowhead; pericyte nucleus is indicated by a double asterisk). **g**, Lack of Mfsd2a expression in choroid plexus vasculature (fourth ventricle coronal view, dashed line), as opposed to the prominent Mfsd2a expression in cerebellar vasculature. $n = 3$ embryos (3 litters per age).

invaginated from the luminal membrane and exocytosed at the abluminal plasma membrane only in *Mfsd2a*$^{-/-}$ mice (Fig. 5d), suggesting that HRP was subject to transcytosis in these animals but not in wild-type littermates (Extended Data Table 2). Together, these findings suggest that the BBB leakiness observed in *Mfsd2a*$^{-/-}$ mice was not caused by opening of tight junctions, but rather by increased transcellular trafficking across the endothelial cytoplasm.

Studies using pericyte-deficient genetic mouse models have shown that pericytes can also regulate BBB integrity. These mice had increased vesicle trafficking without obvious junction defects[4,5], similar to our observations in *Mfsd2a*$^{-/-}$ mice. We therefore examined the possibilities that Mfsd2a may regulate CNS endothelial transcytosis by modulating pericyte function or that the effect of pericytes on endothelial transcytosis is mediated by Mfsd2a. First, pericyte coverage, attachment to the capillary wall, and pericyte ultrastructure and positioning relative to endothelial cells were normal in *Mfsd2a*$^{-/-}$ mice (Extended Data Fig. 6). These data, together with the lack of Mfsd2a expression in pericytes, suggest that the increased transcytosis observed in *Mfsd2a*$^{-/-}$ endothelial cells is not secondary to pericyte abnormalities. Second, a genetic reduction in pericyte coverage can influence endothelial gene expression

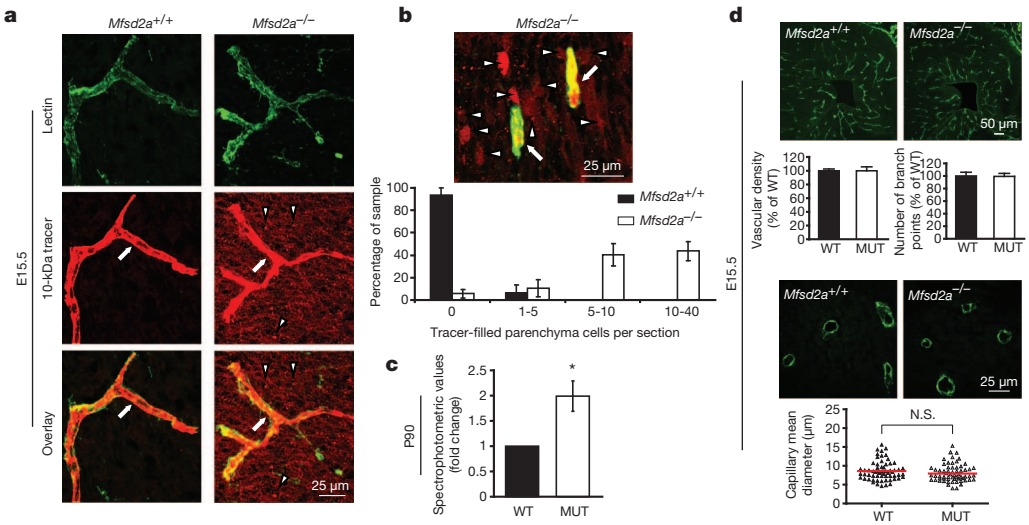

Figure 4 | *Mfsd2a* is required for the establishment of a functional BBB but not for CNS vascular patterning *in vivo*. **a**, **b**, Dextran-tracer (10 kDa) injections at E15.5 revealed a defective BBB in mice lacking *Mfsd2a*. **a**, The tracer was confined to the capillaries (arrow) in wild-type littermates, whereas *Mfsd2a*$^{-/-}$ embryos showed large amounts of tracer leakage in the brain parenchyma (arrowheads). **b**, Capillaries (arrows) surrounded by tracer-filled brain parenchyma cells (arrowheads) in *Mfsd2a*$^{-/-}$ cortex. Quantification of tracer-filled parenchyma cells in control versus *Mfsd2a*$^{-/-}$ cortical plates (bottom panel, $n = 7$ embryos per genotype). **c**, Spectrophotometric quantification of 10-kDa dextran-tracer from cortical extracts of P90 mice, 16 h post intravenous injection, indicating that BBB leakiness in *Mfsd2a*$^{-/-}$ mice persists into adulthood ($n = 3$ mice per genotype). **d**, *Mfsd2a*$^{-/-}$ mice exhibit normal vascular patterning. No abnormalities were found in cortical vascular density, branching and capillary diameter (E15.5; green, PECAM). Quantification of wild-type and *Mfsd2a*$^{-/-}$ samples ($n = 4$ embryos per genotype). All data are mean ± s.e.m. MUT, mutant; N.S., not significant; WT, wild type. *$P < 0.05$ (Mann–Whitney *U*-test).

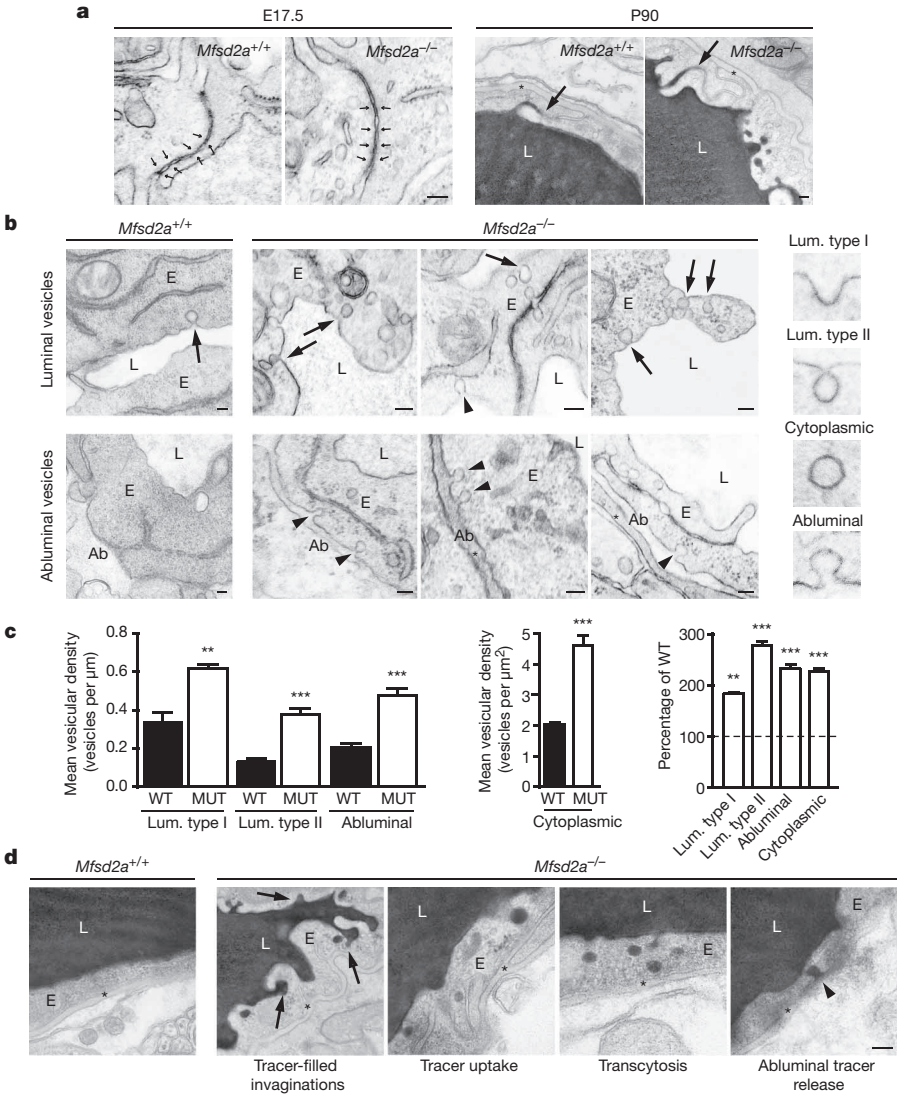

Figure 5 | *Mfsd2a* is required specifically to suppress transcytosis in brain endothelium to maintain BBB integrity. Electron-microscopy examination of BBB integrity. **a**, Embryonic *Mfsd2a*$^{-/-}$ endothelium (E) showed no overt tight-junction ultrastructural defect (left, normal 'kissing points', small arrows). The vessel lumen (L) in HRP-injected adult mice was filled with electron-dense 3-3′ diaminobenzidine (DAB) reaction (black) that diffused into intercellular clefts but stopped sharply at the junction without parenchymal leakage (right, arrows). **b**, Increased vesicular activity in embryonic *Mfsd2a*$^{-/-}$ endothelium (E17.5). Left, wild-type endothelium displayed very few vesicles (arrow). Right, *Mfsd2a*$^{-/-}$ endothelium contained many vesicles of various types: luminal (arrows) and abluminal (Ab; arrowheads) membrane-connected and cytoplasmic vesicles. **c**, Vesicular density quantification (as shown in **b**, reference WT values (dashed line), see also Supplementary Fig. 7a). **d**, Increased transcytosis was evident in HRP-injected adult *Mfsd2a*$^{-/-}$ mice (P90). In wild-type littermates (left) HRP activity was confined to the lumen with no HRP-filled vesicles. Many HRP-filled vesicles found in *Mfsd2a*$^{-/-}$ endothelial cells (right, see quantification in Supplementary Fig. 7b). Luminal invaginations (dye uptake, arrows) and release to the basement membrane (abluminal side, asterisk). Scale bars, 100 nm (**a**, **b**), 200 nm (**c**). All data are mean ± s.e.m. $^{**}P < 0.01$, $^{***}P < 0.001$ (student's *t*-test).

profiles[4,5]. Therefore we analysed published microarray data of two pericyte-deficient mouse models[5] and found a dramatic downregulation of *Mfsd2a* in these mice, with a direct correlation between the reduction of *Mfsd2a* gene expression and the degree of pericyte coverage (Extended Data Fig. 7a). Furthermore, immunostaining for Mfsd2a in *Pdgfb*$^{ret/ret}$ mice[5] revealed a significant decrease in Mfsd2a protein levels in endothelial cells that are not covered by pericytes (Extended Data Fig. 7b–d). Therefore, it is plausible that the increased vesicular trafficking phenotype observed in pericyte-deficient mice is, at least in part, mediated by Mfsd2a, and that endothelial–pericyte interactions control the expression of Mfsd2a, which in turn controls BBB integrity.

We demonstrate that Mfsd2a is required to suppress endothelial transcytosis in the CNS. Because of Mfsd2a's involvement in human trophoblast cell fusion[24] and of our genetic evidence for its role in suppressing transcytosis, we propose that Mfsd2a serves as a cell-surface molecule to regulate membrane fusion or trafficking. Indeed, from immuno-electron-microscopy examination, Mfsd2a protein was found in the luminal plasma membrane and associated with vesicular structures in cerebral endothelial cells, but not in tight junctions (Extended Data Fig. 8). At present, it is not clear whether the reported transporter function of Mfsd2a is related to its role in BBB formation.

BBB breakdown has been reported in the aetiology of various neurological disorders[7–10], and two separate *Mfsd2a*-deficient mouse lines were reported to exhibit neurological abnormalities, such as ataxic behaviour[21,25]. Finding a novel physiological role of Mfsd2a may provide a valuable tool to address how a non-functional BBB could affect brain development. In addition, our finding also highlights the importance of the transcytotic mechanism in BBB function, whereas most previous attention has been focused on potential BBB leaks through intercellular junctions. Indeed, increased numbers of pinocytotic vesicles were observed following acute exposure to external stress inducers in animal models[26], and have also been observed in human pathological conditions[9]. It will

be interesting to examine whether Mfsd2a is involved in these pathological and acute assault situations. We cannot be certain that the elevated levels of transcytosis in *Mfsd2a*$^{-/-}$ mice were not due to some form of acute cellular stress, but it is very unlikely. This is because under stress, either cells respond to restore homeostasis or cell death occurs[27]. However, increased transcytosis in *Mfsd2a*$^{-/-}$ mice persists from embryonic stages to adulthood, and up to 6 months of age these mice exhibit no sign of vascular degeneration (Extended Data Fig. 5c). Our identification of a key molecular player in BBB formation may also aid efforts to develop therapeutic approaches for efficient drug delivery to the CNS. As an accessible cell surface molecule, Mfsd2a is poised to be a potential therapeutic target for BBB restoration and manipulation.

METHODS SUMMARY

The lowest volume of 10-kDa dextran tetramethylrhodamine, lysine fixable (D3312 Invitrogen) that still facilitated full perfusion was injected into the embryonic liver, while keeping the embryo connected to the maternal blood circulation through the umbilical cord. After 3 minutes of tracer circulation, embryonic heads were fixed by immersion in 4% paraformaldehyde (PFA) overnight at 4 °C, cryopreserved in 30% sucrose and frozen in TissueTek OCT (Sakura). Sections of 12 μm were then collected and post-fixed in 4% PFA at room temperature (20–25 °C) for 15 min, washed in PBS and co-stained with either α-PECAM antibody or with isolectin B4 to visualize blood vessels (see Methods for details). P90 HRP injection and E17.5 cortex capillaries transmission electron microscopy (TEM) imaging was done as described previously[2].

Online Content Any additional Methods, Extended Data display items and Source Data are available in the online version of the paper; references unique to these sections appear only in the online paper.

Received 27 September 2013; accepted 14 April 2014.
Published online 14 May 2014.

1. Saunders, N. R., Liddelow, S. A. & Dziegielewska, K. M. Barrier mechanisms in the developing brain. *Front. Pharmacol.* **3,** 46 (2012).
2. Reese, T. S. & Karnovsky, M. J. Fine structural localization of a blood-brain barrier to exogenous peroxidase. *J. Cell Biol.* **34,** 207–217 (1967).
3. Siegenthaler, J. A., Sohet, F. & Daneman, R. 'Sealing off the CNS': cellular and molecular regulation of blood-brain barriergenesis. *Curr. Opin. Neurobiol.* **23,** 1057–1064 (2013).
4. Daneman, R., Zhou, L., Kebede, A. A. & Barres, B. A. Pericytes are required for blood–brain barrier integrity during embryogenesis. *Nature* **468,** 562–566 (2010).
5. Armulik, A. *et al.* Pericytes regulate the blood–brain barrier. *Nature* **468,** 557–561 (2010).
6. Bell, R. D. *et al.* Pericytes control key neurovascular functions and neuronal phenotype in the adult brain and during brain aging. *Neuron* **68,** 321–323 (2010).
7. Zlokovic, B. V. The blood-brain barrier in health and chronic neurodegenerative disorders. *Neuron* **57,** 178–201 (2008).
8. Zhong, Z. *et al.* ALS-causing SOD1 mutants generate vascular changes prior to motor neuron degeneration. *Nature Neurosci.* **11,** 420–422 (2008).
9. Bell, R. D. & Zlokovic, B. V. Neurovascular mechanisms and blood-brain barrier disorder in Alzheimer's disease. *Acta Neuropathol.* **118,** 103–113 (2009).
10. Bell, R. D. *et al.* Apolipoprotein E controls cerebrovascular integrity via cyclophilin A. *Nature* **485,** 512–516 (2012).
11. Saunders, N. R. *et al.* Transporters of the blood–brain and blood–CSF interfaces in development and in the adult. *Mol. Aspects Med.* **34,** 742–752 (2013).
12. Stenman, J. M. *et al.* Canonical Wnt signaling regulates organ-specific assembly and differentiation of CNS vasculature. *Science* **322,** 1247–1250 (2008).
13. Liebner, S. *et al.* Wnt/β-catenin signaling controls development of the blood–brain barrier. *J. Cell Biol.* **183,** 409–417 (2008).
14. Daneman, R. *et al.* Wnt/β-catenin signaling is required for CNS, but not non-CNS, angiogenesis. *Proc. Natl Acad. Sci. USA* **106,** 641–646 (2009).
15. Tam, S. J. *et al.* Death receptors DR6 and TROY regulate brain vascular development. *Dev. Cell* **22,** 403–417 (2012).
16. Cullen, M. *et al.* GPR124, an orphan G protein-coupled receptor, is required for CNS-specific vascularization and establishment of the blood–brain barrier. *Proc. Natl Acad. Sci. USA* **108,** 5759–5764 (2011).
17. Wang, Y. *et al.* Norrin/Frizzled4 signaling in retinal vascular development and blood brain barrier plasticity. *Cell* **151,** 1332–1344 (2012).
18. Alvarez, J. I. *et al.* The Hedgehog pathway promotes blood-brain barrier integrity and CNS immune quiescence. *Science* **334,** 1727–1731 (2011).
19. Mizee, M. R. *et al.* Retinoic acid induces blood–brain barrier development. *J. Neurosci.* **33,** 1660–1671 (2013).
20. Stern, L., Rapoport, J. L. & Lokschina, E. S. Le fonctionnement de la barrière hémato-encéphalique chez les nouveau-nés. *C. R. Soc. Biol* **100,** 231–223 (1929).
21. Tang, T. *et al.* A mouse knockout library for secreted and transmembrane proteins. *Nature Biotechnol.* **28,** 749–755 (2010).
22. Esnault, C. placenta-specific receptor for the fusogenic, endogenous retrovirus-derived, human syncytin-2. *Proc. Natl Acad. Sci. USA* **105,** 17532–17537 (2008).
23. Reiling, J. H. *et al.* A Haploid genetic screen identifies the major facilitator domain containing2A (MFSD2A) transporter as a key mediator in the response to tunicamycin. *Proc. Natl Acad. Sci. USA* **108,** 11756–11765 (2011).
24. Toufaily, C. *et al.* MFSD2a, the Syncytin-2 receptor, is important for trophoblast fusion. *Placenta* **34,** 85–88 (2013).
25. Berger, J. H. Charron, M.J. Silver, D.L. Major facilitator superfamily domain-containing protein 2a (MFSD2A) has roles in body growth, motor function, and lipid metabolism. *PLoS One* **7,** e50629 (2012).
26. Nag, S. In *The Blood–Brain Barrier—Biology and Research Protocols.* Part 2 (ed. Nag, S.) 99–100 (2003).
27. Chen, F., Evans, A., Pham, J. & Plosky, B. (eds) *Mol. Cell* Special Review issue **40** (2010).

Supplementary Information is available in the online version of the paper.

Acknowledgements We thank M. Karnovsky, E. Raviola and T. Reese for advice and discussion; S. R. Datta, C. Weitz, M. Greenberg, Q. Ma, C. Harvey and members of the Gu laboratory for comments on the manuscript; D. Sabatini and J. Reeling for sharing unpublished data; C. Betsholtz and C. Olsson for providing *Pdgfb*$^{ret/ret}$ mouse brain samples; T. Schwarz and A. Oztan for discussion and advice on cell trafficking; W.-J. Oh for help with graphic illustrations; the Flow Cytometry Facility in the department of Systems Biology at Harvard Medical School for cell sorting; the Microarray Core at Dana-Farber Cancer Institute for Affymetrix assay; HSPH Bioinformatics Core, Harvard School of Public Health, for assistance with microarray analysis and Gene Expression Omnibus (GEO) submission; the Enhanced Neuroimaging Core at Harvard NeuroDiscovery Center for helping with confocal imaging and image analysis; the HMS Electron Microscopy Core Facility, the Neurobiology Imaging Facility for consultation and instrument availability that supported this work (this facility is supported in part by the Neural Imaging Center as part of an NINDS P30 Core Center grant no. NS072030); R. Polakiewicz and J. Xie from CST for generating Mfsd2a antibodies. This work was supported by the Harold Perlman postdoctoral fellowships, the Goldenson postdoctoral fellowship, and the Lefler postdoctoral fellowship (A.B.-Z.); the DFG-German Research Foundation postdoctoral fellowship (E.K.); the Mahoney postdoctoral fellowship (B.L.); NIH training grant 5T32MH20017-15 (B.J.A.); and the Sloan research fellowship, Armenise junior faculty award, the Genise Goldenson fund, the Freudenberger award, and NIH grant R01NS064583 (C.G.).

Author Contributions C.G. and A.B.-Z. conceived and designed the project. A.B.-Z, B.L., E.K, B.J.A. and H.Y. performed experiments. A.B.-Z. and B.L. analysed data and preformed image analysis and quantification. Y.M. analysed microarray data. C.G. and A.B.-Z. wrote the manuscript with significant input from B.L. and B.J.A.

Author Information Microarray data have been deposited in NCBI's Gene Expression Omnibus (http://www.ncbi.nlm.nih.gov/geo/) and are accessible through GEO series accession number GSE56777. Reprints and permissions information is available at www.nature.com/reprints. The authors declare no competing financial interests. Readers are welcome to comment on the online version of the paper. Correspondence and requests for materials should be addressed to C.G. (chenghua_gu@hms.harvard.edu).

METHODS

Animals. Wild-type Swiss-Webster mice (Taconic Farms) were used for embryonic BBB functionality assays and expression profiles. Homozygous *Tie2-GFP* transgenic mice (Jackson laboratory, strain 003658) were used for BBB transcriptional profiling. *Mfsd2a*-null mice[21] (Mouse Biology Program, University of California, Davis —MMRRC strain 032467-UCD, B6;129S5-Mfsd2atm1Lex/Mmucd) were maintained on C57Bl/6;129SVE mixed background and used for testing the involvement of Mfsd2a in barrier genesis. *Mfsd2a*-null mutant mice were genotyped using the following PCR primers: 5′-CCTGGTTTGCTAAGTGCTAGC-3′ and 5′-GTTCACTGGCTTGGAGGATGC-3′, which provide a 210-bp product for the *Mfsd2a* wild-type allele; and 5′-CACTTCCTAAAGCCTTACTTC-3′ and 5′-GC AGCGCATCGCCTTCTATC-3′, which provide a 301-bp product for the *Mfsd2a*-knockout allele.

Pregnant mice were obtained following overnight mating (day of vaginal plug was defined as embryonic day 0.5).

All animals were treated according to institutional and US National Institutes of Health (NIH) guidelines approved by the Institutional Animal Care and Use Committee (IACUC) at Harvard Medical School.

Immunohistochemistry. Tissues were fixed with 4% paraformaldehyde (PFA) at 4 °C overnight, cryopreserved in 30% sucrose and frozen in TissueTek OCT (Sakura). Tissue sections were blocked with 5% goat serum, permeabilized with 0.5% Triton X-100, and stained with the following primary antibodies: α-PECAM (1:500; 553370, BD PharmingenTM), α-Claudin5 (1:400; 35-2500, Invitrogen), α-Mfsd2a (1:500; Cell Signaling Technologies (under development)), α-Pdgfrβ (1:100; 141402, eBioscience), α-CD31 (1:100; 558744, BD PharmingenTM), α-SMA (1:100; C6198, Sigma Aldrich), followed by 568/488 Alexa Fluor-conjugated secondary antibodies (1:300–1:1000, Invitrogen) or with Isolectin B4 (1:500; I21411, Molecular Probes). Slides were mounted in Fluoromount G (EMS) and visualized by epifluorescence, light, or confocal microscopy.

***In situ* hybridization.** Tissue samples were frozen in liquid nitrogen and embedded in TissueTek OCT (Sakura). Sections (18 μm) were hybridized with a digoxigenin (DIG)-labelled mouse *Mfsd2a* antisense riboprobe (1,524–2,024 bp NM_029662) at 60 °C overnight. A sense probe was used to ensure signal specificity. For detection, signals were developed using anti-DIG antibody conjugated with alkaline phosphatase (Roche). After antibody treatment, sections were incubated with BM Purple AP Substrate (Roche).

Embryonic BBB permeability assay. The method is based on the well-established adult BBB dye-injection assay with special considerations for the injection site and volume to cater the nature of embryonic vasculature[20,28–30].

Four major modifications were made: first, embryos were injected while still attached via the umbilical cord to the mother's blood circulation, minimizing abrupt changes in blood flow. Deeply anaesthetized pregnant mice were used.

Second, taking advantage of the sinusoidal, fenestrated and most permeable liver vasculature, dye was injected using a Hamilton syringe into the embryonic liver and was taken into the circulation in a matter of seconds.

Third, dye volume was adjusted to a minimum that still allows detection in all CNS capillaries after 3 min of circulation. High-fluoresce-intensity dye enables the use of small volumes and facilitates detection at the single-capillary level (10-kDa dextran-tetramethylrhodamine, lysine fixable, 4 mg ml^{-1} (D3312 Invitrogen), 1 μl for E13.5, 2 μl for E14.5, 5 μl for E15.5).

Fourth, traditional perfusion fixation was omitted, again to prevent damage to capillaries. Instead, fixable dyes were used to allow reliable immobilization of the dye at the end of the circulation time (relatively small embryonic brain facilitates immersion fixation).

Embryonic heads were fixed by immersion in 4% PFA overnight at 4 °C, cryopreserved in 30% sucrose and frozen in TissueTek OCT (Sakura). Sections of 12 μm were then collected and post-fixed in 4% PFA at room temperature for 15 min, washed in PBS and co-stained with either α-PECAM antibody or with isolectin B4 to visualize blood vessels. All embryos from each litter were injected blind before genotyping.

Postnatal and adult BBB permeability assay. P2–P5 pups were deeply anaesthetized and three methods were used: the first method involved injection of 10 μl of 10-kDa or 70-kDa dextran tetramethylrhodamine (4 mg ml^{-1} D3312 Invitrogen) into the left ventricle with a Hamilton syringe. After 5 min of circulation, brains were dissected and fixed by immersion in 4% PFA at 4 °C overnight, cryopreserved in 30% sucrose and frozen in TissueTek OCT (Sakura). Sections of 12 μm were collected and post-fixed in 4% PFA at room temperature for 15 min, washed in PBS and co-stained to visualize blood vessels with either α-PECAM primary antibody (1:500; 553370, BD Pharmingen), followed by 488-Alexa Fluor conjugated secondary antibody (1:1000, Invitrogen) or with isolectin B4 (1:500; I21411, Molecular Probes).

The second method involved injection of 10 μl of HRP type II (5 mg ml^{-1} P8250-50KU Sigma-Aldrich) into the left heart ventricle with a Hamilton syringe. After 5 min of circulation brains were dissected and immersion fixed in 2% glutaraldehyde in 4% PFA in cacodylate buffer (0.1 M, pH 7.3) at room temperature for 1 h then at 4 °C for 3 h then washed in cacodylate buffer overnight. Cortical-vibratome sections (100 μm) were processed in a standard DAB reaction.

The third method involved the use of EZ-link NHS-sulfo-biotin as a tracer, as described previously[17].

Imaging. Nikon Eclipse 80i microscope equipped with a Nikon DS-2 digital camera was used to image HRP tracer experiments, vasculature density and pericyte coverage comparisons and expression analyses. Zeiss LSM 510 META upright confocal microscope was used to image Dextran and NHS-sulfo-biotin BBB permeability assays. A Nikon FluoView FV1000 laser scanning confocal microscope and a Leica SP8 laser scanning confocal microscope were used for imaging Mfsd2a and pericyte marker immunohistochemistry. Images were processed using Adobe Photoshop and ImageJ (NIH).

Morphometric analysis of vasculature. Coronal sections (25-μm thick) of E15.5, P4 and P70 brains were immunostained for PECAM. For vascular density and branching, confocal images were acquired with a Nikon FluoView FV1000 laser scanning confocal microscope and maximal projection images (5 per animal) were used for quantifications. The number of branching points was manually counted. Capillary density was quantified using MetaMorph software (Universal Imaging, Downingtown, Pennsylvania) by measuring the area occupied by PECAM-positive vessels per cortical area. The mean capillary diameter was measured manually in ImageJ from cross-sectional vascular profiles (20 per animal) on micrographs (5–7 per animal) taken under a ×60 objective with a ×2 digital zoom.

For artery distribution quantification, 25-μm-thick sections (P60) were stained for smooth muscle actin (SMA) and PECAM. The proportion of PECAM-positive brain vessels with artery (SMA) identity was quantified using MetaMorph and expressed as percent of controls. Quantification was carried out blind.

Quantification of cortical-vessel pericyte coverage. Pericyte coverage of cortex vessels in *Mfsd2a*$^{-/-}$ and wild-type littermate control mice was quantified by analysing the proportion of total claudin-5-positive endothelial length also positive for the pericyte markers CD13 or Pdgfrβ. Immunostaining was performed on 20-μm sections of P5 cortex. In each animal, 20 images of 10 different sections were analysed. Microvasculature was found to be completely covered by pericytes in both control and *Mfsd2a*$^{-/-}$ mice and therefore no error bars are presented for the average pericyte coverage in Extended Data Fig. 6a, b ($n = 3$). All the analysis was done with ImageJ (NIH). Quantification was carried out blind.

Quantification of vessel leakage. Epifluorescence images of sections from injected tracer and co-stained with lectin were analysed manually with ImageJ (NIH). Coronal cortical sections (12 μm) of the same rostrocaudal position were used for the analysis. The same acquisition parameters were applied to all images and the same threshold was used. Tracer-positive cells found outside a vessel (parenchyma) were used as a parameter for leakage. For each embryo, at least 20 sections of a fixed lateral cortical plate area were scored. Four arbitrary leakage groups were classified based on the number of tracer parenchyma positive cells per section (0, 1–5, 5–10 and 10–40). Average representation of each leakage group was calculated for *Mfsd2a*$^{-/-}$ and control embryos. Quantification was carried out blind.

Spectrophotometric quantification of 10-kDa fluoro-ruby-dextran tracer was carried out from cortical extracts, 16 h after tail-vein injections in adult mice, as described previously[5].

Transmission electron microscopy. TEM imaging of P90 HRP injection and E17.5 cortex capillaries was carried out as described previously[2]. HRP (10 mg (per 20 g); Sigma Aldrich, HRP type II) were dissolved in 0.4 ml of PBS and injected into the tail veins of deeply anaesthetized P90 mice. After 30 min of HRP circulation, brains were dissected and fixed by immersion in a 0.1 M sodium-cacodylate-buffered mixture (5% glutaraldehyde and 4% PFA) for 1 h at room temperature followed by 5 h in PFA at 4 °C. Following fixation, the tissue was washed overnight in 0.1 M sodium-cacodylate buffer and then cut in 50-μm-thick free-floating sections using a vibrotome. Sections were incubated for 45 min at room temperature in 0.05 M Tris-HCl pH 7.6 buffer, containing 5.0 mg per 10 ml of 3-3′ diaminobenzidine (DAB, Sigma Aldrich) with 0.01% hydrogen peroxide. Sections were then post-fixed in 1% osmium tetroxide and 1.5% potassium ferrocyanide and dehydrated and embedded in epoxy resin. E17.5 samples were processed as the P90 samples without HRP injection and with longer fixation times (2–3 days in room temperature). Ultrathin sections (80 nm) were then cut from the block surface, collected on copper grids, stained with Reynold's lead citrate and examined under a 1200EX electron microscope (JEOL) equipped with a 2k CCD digital camera (AMT).

Immunogold labelling for electron microscopy. Mice were deeply anaesthetized and perfused through the heart with 30 ml of PBS followed by 150 ml of a fixative solution (0.5% glutaraldehyde in 4% PFA prepared in 0.1 mM phosphate buffer, pH 7.4), and then by 100 ml of 4% PFA in phosphate buffer. The brain was removed and post fixed in 4% PFA (30 min, 4 °C) and washed in PBS. Coronal brain sections (50-μm thick) were cut on the same day with a vibratome and processed free floating.

Sections were immersed in 0.1% sodium borohydride in PBS (20 min, room temperature), rinsed in PBS and pre-incubated (2 h) in a blocking solution of PBS containing 10% normal goat serum, 0.5% gelatine and 0.01% Triton. Incubation (24 h, 20–25 °C) with rabbit anti-Mfsd2a (1:100; Cell Signaling Technologies (under development)) primary antibody was followed by rinses in PBS and incubation (overnight, 20–25 °C) in a dilution of gold-labelled goat anti-rabbit IgGs (1:50; 2004, Nanoprobes). After washes in PBS and sodium acetate, the size of immunogold particles was silver-enhanced and sections rinsed in phosphate buffer before processing for electron microscopy.

Statistical analysis. Comparison between wild-type and *Mfsd2a*$^{-/-}$ pericyte coverage and spectrophotometric quantification of 10-kDa fluoro-ruby-dextran tracer leakage was performed by a Mann–Whitney *U*-test (appropriate for small sample size; each embryo was considered as a sample). An unpaired student's *t*-test was used (GraphPad Prism 4 Software) for comparison between wild-type and *Mfsd2a*$^{-/-}$ for vascular density, artery distribution, number of vesicular types, mean capillary diameter and Mfsd2a expression in pericyte deficient mice. $P < 0.05$ was considered significant (StatXact Cytel Software Corporation,Cambridge, Massachusetts, USA).

Transcriptional profiling. E13.5 *Tie2-GFP* embryos were micro-dissected for cortex and lungs. Cortex tissue was carefully cleared of the meninges and choroid plexus. FACS purification of GFP-positive cells and GeneChip analysis was performed as described previously[31]. RNA was purified with Arcturus PicoPure RNA isolation kit (Applied biosystems), followed by NuGEN Ovation V2 standard linear amplification and hybridization to Affymetrix Mouse Genome 430 2.0 Array. All material from a single litter (10–13 embryos) was pooled and considered as a biological replicate. Four biological replicates were used. Each biological replicate represents purification from different litters performed on different days.

Transcriptional profile analysis of pericyte deficient mice. Expression data from a published study of pericyte-deficient mice[5] were obtained from the Gene Expression Omnibus (http://www.ncbi.nlm.nih.gov/geo, accession number GSE15892). All microarrays were analysed using the MAS5 probe set condensation algorithm with Expression Console software (Affymetrix). P values were determined using a two-tailed student's *t*-test ($n = 4$).

Mfsd2a protein expression in *Pdgfb*$^{ret/ret}$ mice. Brain samples from P10–P14 mice and controls were kindly provided by C. Betsholtz. Sample processing and immunohistochemistry was carried out as described for all other samples in our study. Mfsd2a staining quantification was carried out with 12-μm cortical sagittal sections. Confocal images were acquired with a Nikon FluoView FV1000 laser scanning confocal microscope. Quantification of mean grey value per vascular profile was done with ImageJ (NIH) by outlining vascular profiles according to lectin staining and measuring Mfsd2a intensity in these areas. In all images, Pdgfrβ antibody staining was used to test presence of pericytes in quantified vessels. $n = 2$ animals per genotype, 60 images quantified of at least 600 vascular profiles per animal. Quantification was carried out blind.

28. Ek, C. J., Habgood, M. D., Dziegielewska, K. M. & Saunders, N. R. Functional effectiveness of the blood-brain barrier to small water-soluble molecules in developing and adult opossum (Monodelphisdomestica). *J. Comp. Neurol.* **496,** 13–26 (2006).
29. Risau, W., Hallmann, R. & Albrecht, U. Differentiation-dependent expression of proteins in brain endothelium during development of the blood-brain barrier. *Dev. Biol.* **117,** 537–545 (1986).
30. Bauer, H. *et al.* Ontogenic expression of the erythroid-type glucose transporter (Glut 1) in the telencephalon of the mouse: correlation to the tightening of the blood-brain barrier. *Brain Res. Dev. Brain Res.* **86,** 317–325 (1995).
31. Daneman, R. *et al.* The mouse blood-brain barrier transcriptome: a new resource for understanding the development and function of brain endothelial cells. *PLoS One* **5,** 313741 (2010).

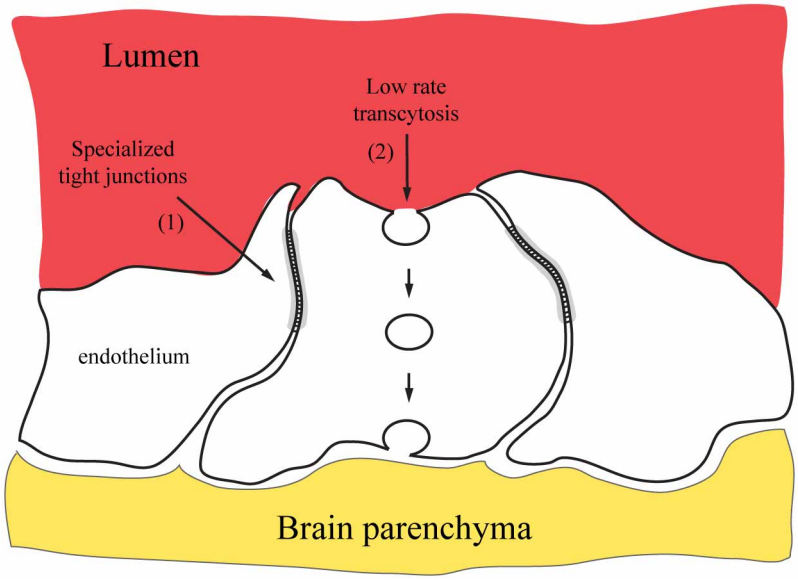

Extended Data Figure 1 | Diagram illustrating two unique BBB properties of CNS endothelial cells. Compared to the endothelial cells from the rest of the body, CNS endothelial cells that possess a BBB are characterized by highly specialized tight junctions sealing the space between adjacent cells (1), and an unusually low rate of transcytosis from the vessel lumen to the brain parenchyma (2).

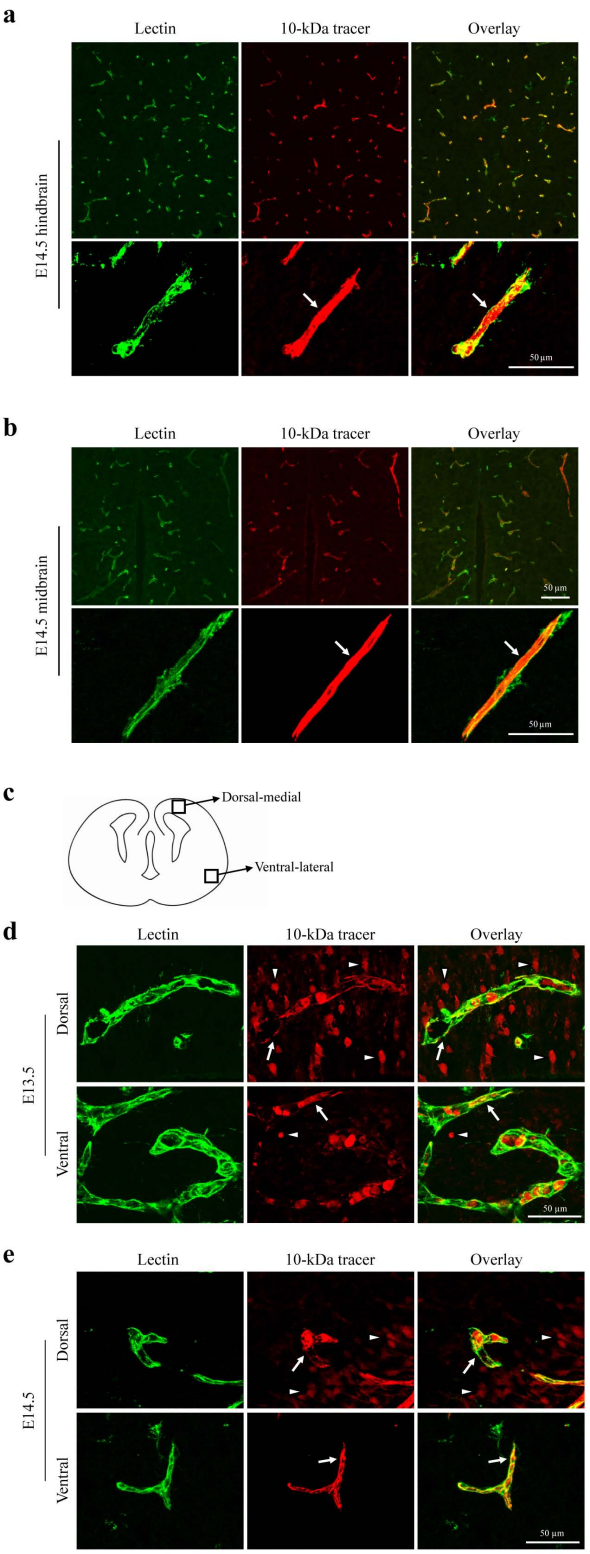

Extended Data Figure 2 | Spatial and temporal BBB maturation across brain regions and cortical regions. **a**, **b**, Embryonic BBB develops in a caudal-to-rostral spatial pattern. Dextran-tracer (10 kDa) injection revealed that the BBB is already functional in the hindbrain (**a**) and midbrain (**b**) at E14.5, a time-point at which cortical BBB is still leaky. Epifluorescence (low magnification) and confocal (high magnification) images of brain sections from injected embryos are shown. As illustrated in both **a** and **b**, tracer was confined to blood vessels (arrows). **c–e**, Cortical BBB develops in a ventrolateral to dorsomedial spatial pattern. **c**, Diagram of the embryonic cortex indicating dorsal–medial and ventral–lateral cortical regions illustrated in **d** and **e**. **d**, At E13.5, the BBB of the dorsal cortex (top panels) is not fully formed, as evidenced by little tracer inside the blood vessels (arrow) and tracer-filled parenchymal cells (arrowheads). In the ventral cortex (bottom panels), capillaries were better sealed, showing more tracer within the lumen (arrow) and less tracer in the brain parenchyma (arrowhead). **e**, At E14.5, the capillaries in the dorsal cortex (top panels) were still leaky, with little tracer inside the capillaries (arrow) and tracer-stained surrounding parenchyma (arrowheads). At the same age, the BBB of the ventral cortex (bottom panels) was already functional, with all tracer confined to the capillaries (arrow). Green, lectin; red, 10-kDa tracer. $n = 6$ embryos from 3 litters for each age.

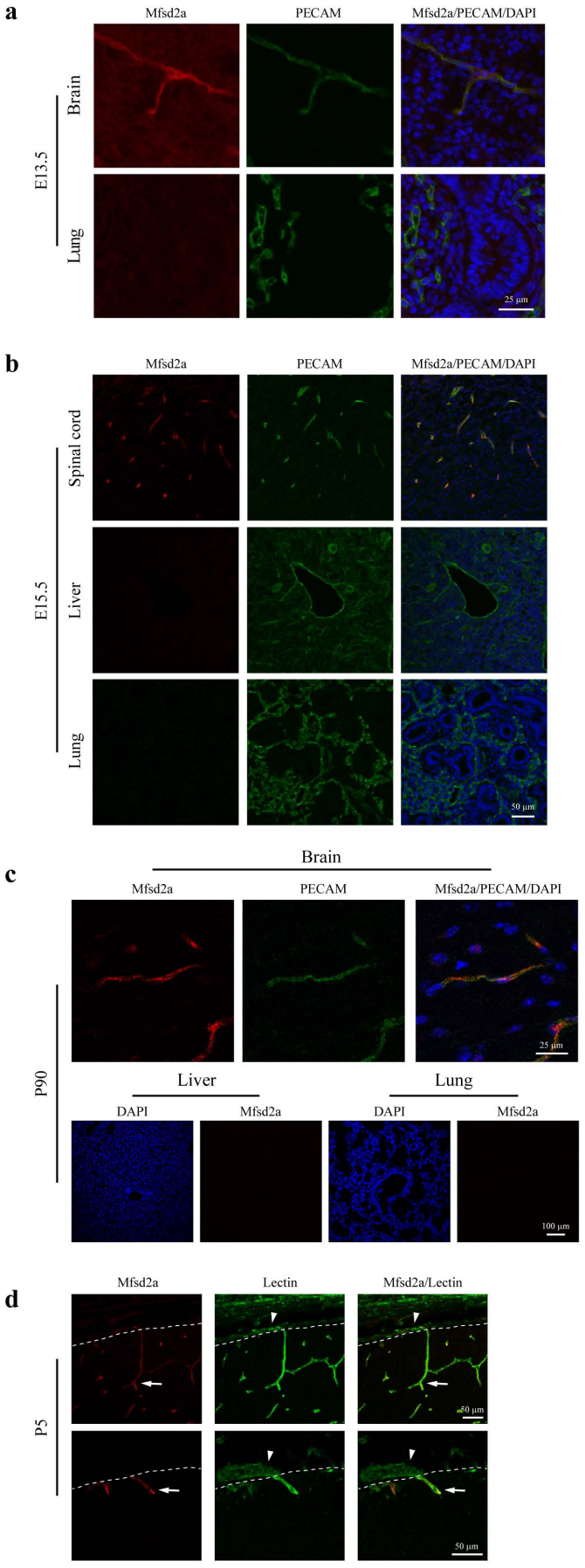

Extended Data Figure 3 | Mfsd2a protein is selectively expressed in BBB-containing CNS vasculature of both embryos and adults. Immunohistochemical staining of Mfsd2a protein demonstrating its specific expression in BBB-containing CNS vasculature. Red, Mfsd2a; green, PECAM (endothelium); blue, DAPI (nuclei). **a**, At E13.5, the time of BBB establishment, Mfsd2a expression was detected in the brain (top panels) but not in the lung vessels (bottom panels), confirming the microarray data. **b**, At E15.5,the first developmental time-point of BBB functionality, Mfsd2a expression was detected in spinal cord (top panels) but not in lung (middle panels) or liver vessels (bottom panels). **c**, Mfsd2a selective expression in BBB-containing vessels persists in adult mice (P90) as shown in brain vessels (top panels) but not in lung or liver (bottom panels). **d**, Mfsd2a is expressed in cerebral vessel (arrow) but not in pial vessels (arrow heads). Low (top panel) and high magnification (bottom panel) of pial-cerebral boundary (dotted line) of P5 dorsal cortex (wild-type mice). $n = 3$ embryos from 3 litters for each age.

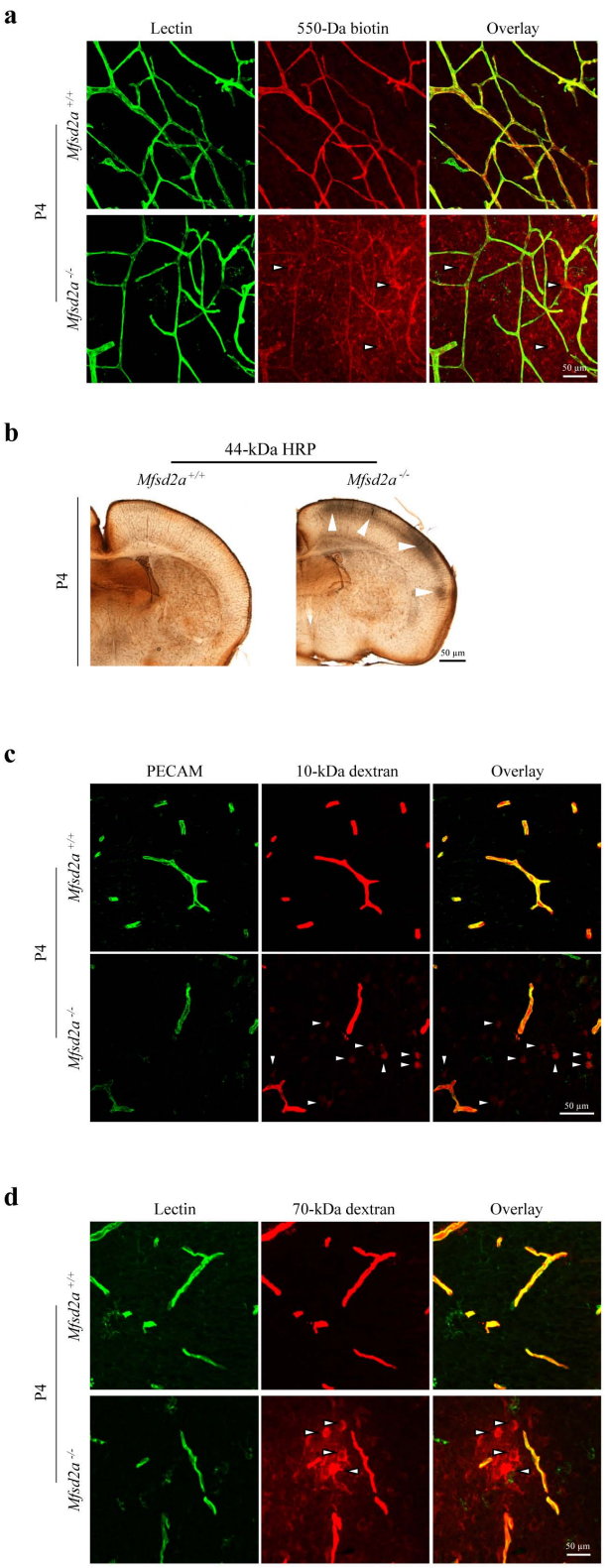

Extended Data Figure 4 | The leaky BBB phenotype in *Mfsd2a*$^{-/-}$ mice persists after birth and is not restricted to carbohydrate-based tracers. **a**, **b**, Injection of two non-carbohydrate-based tracers with different molecular weight and different molecular compositions at P4 revealed a persistent leaky barrier phenotype in mice lacking *Mfsd2a*. **a**, The small-molecular-weight tracer sulfo-NHS-biotin (~550 Da), was confined to vessels in wild-type controls (upper panels), whereas it leaked out of the vessels (arrowheads) in *Mfsd2a*$^{-/-}$ mice (lower panels). Green, lectin; red, tracer. **b**, The high-molecular-weight protein tracer HRP (~44 kDa) was confined to vessels in control mice at P4 (left), whereas in mice lacking *Mfsd2a* (right), tracer was diffusing into the brain parenchyma (arrowheads). Brown, visualization of HRP in light microscopy by DAB reaction. Stainings were carried out on 100-µm cortical sections of tracer-injected animals. $n = 4$ pups per genotype from 3 litters. **c**, **d**, BBB leakage of tracer with 70 kDa molecular weight is observed in postnatal *Mfsd2a*$^{-/-}$ mice. Green, lectin or PECAM (vessels); red, tracer. The 10-kDa (**a**) and 70-kDa (**b**) tracers fluoro-ruby-dextran were confined to vessels in control mice (top panels), but not in *Mfsd2a*$^{-/-}$ mice (bottom panels), where tracer was taken up by brain parenchymal cells (arrowheads). Stainings were carried out on 12-µm cortical sections of tracer-injected animals. $n = 3$ pups per genotype from 3 litters.

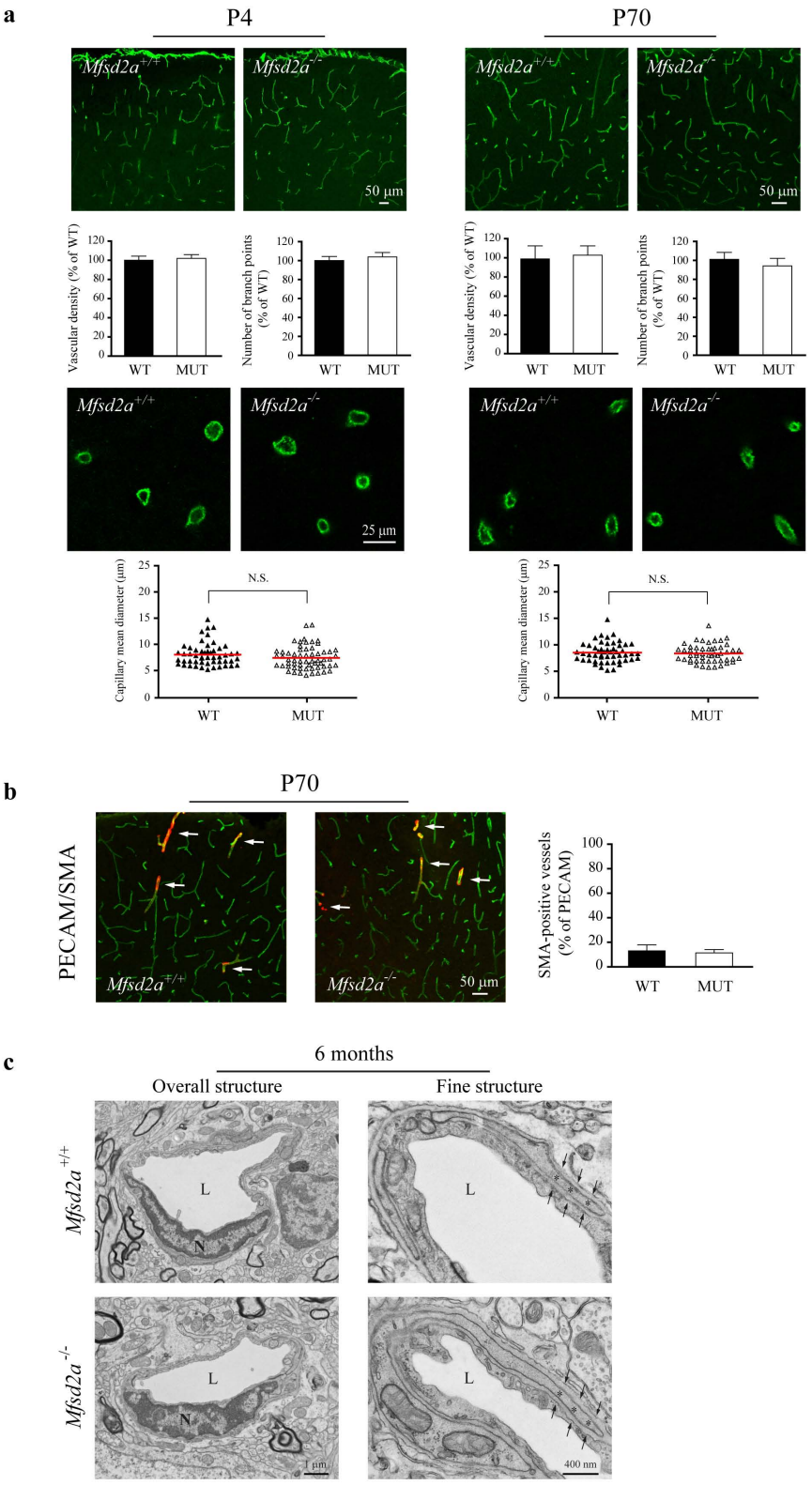

Extended Data Figure 5 | Perinatal and adult mice lacking *Mfsd2a* do not display changes in cerebrovascular network properties or signs of vascular degeneration. **a**, No abnormalities were found in cortical capillary density and vascular branching (top panels) as well as capillary diameter (bottom panels) of postnatal (P4, left) and adult (P70, right) *Mfsd2a*$^{-/-}$ mice. Images of vascular staining in coronal cortical sections and high-magnification images of cross-section profiles of capillaries (green, PECAM) and quantification. Data are mean ± s.e.m. $n = 3$ animals per genotype, 20 sections per animal. **b**, Immunostaining for smooth-muscle actin (arterial identifier, arrows) revealed no abnormalities in arterial distribution and specification in *Mfsd2a*$^{-/-}$ mice. Images of coronal cortical sections (left, green, PECAM; red, SMA) and quantification (right). Data are mean ± s.e.m. $n = 3$ animals per genotype, 20 sections per animal. **c**, Electron-microscopy examination of older *Mfsd2a*$^{-/-}$ mice did not reveal signs of cerebrovascular degeneration. Left, the overall capillary structure (for example, cell size, shape of the nucleus, thickness of the vessel wall, basement membrane integrity and pericyte attachment) did not differ between wild-type and mutant mice. Right, at higher magnification, normal features, such as pericyte (asterisk) attachment within a normal basement membrane (between arrows), could be observed in mice lacking *Mfsd2a*.

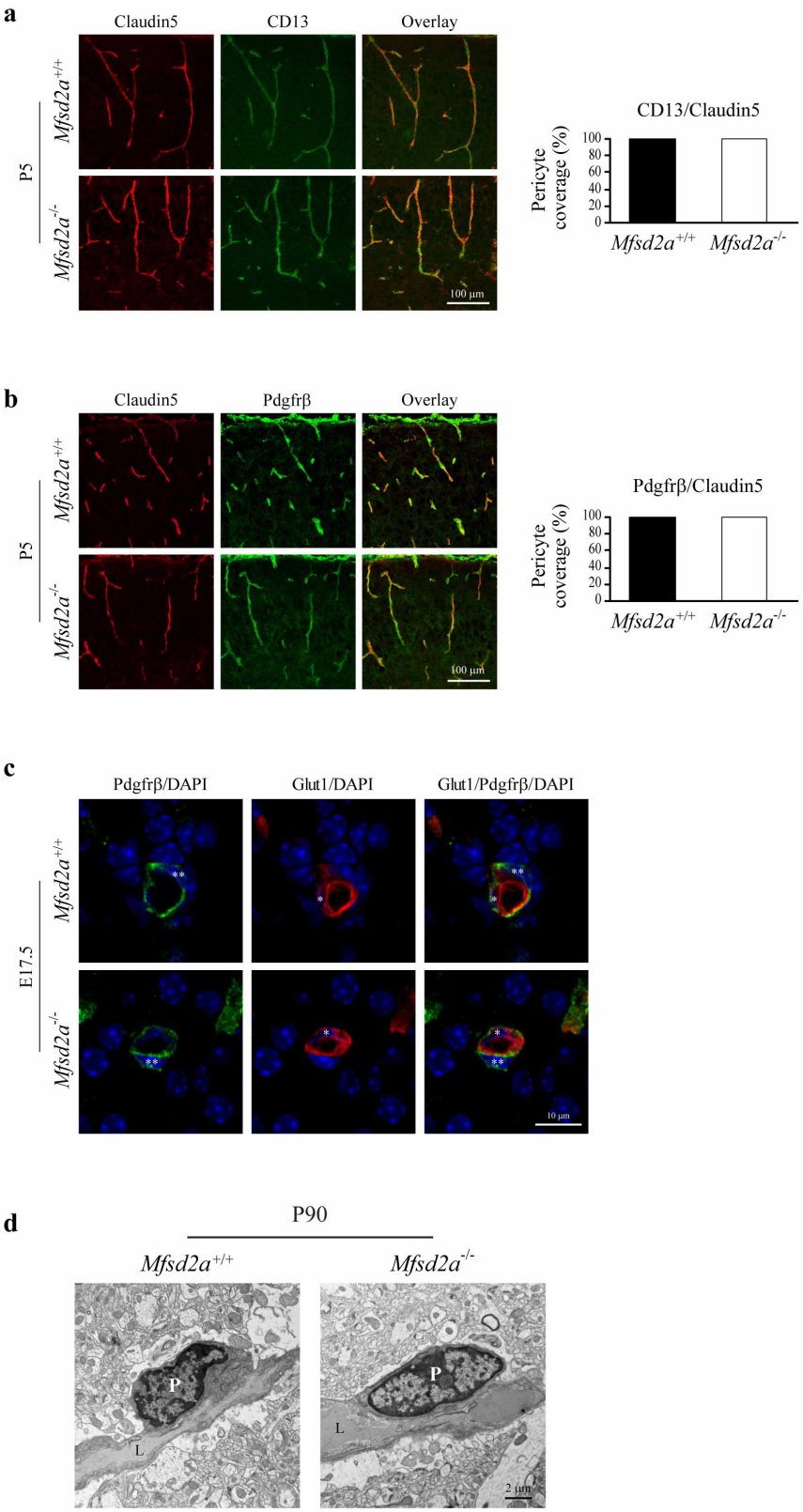

Extended Data Figure 6 | Pericyte coverage, attachment and ultrastructure are normal in *Mfsd2a*$^{-/-}$ mice. **a**, **b**, *Mfsd2a*$^{-/-}$ mice exhibit normal pericyte coverage. Co-staining of endothelium (claudin-5, red) and pericytes (CD13 in **a** and Pdgfrβ in **b**, green) revealed no overt difference in pericyte coverage of dorsal cortex vessels between wild-type (top row) and *Mfsd2a*$^{-/-}$ (bottom row) mice at P5. Quantification of vascular coverage in both **a** and **b** showed no significant difference between wild-type and *Mfsd2a*$^{-/-}$ samples ($P > 0.5$). Data are mean ± s.e.m. $n = 3$ pups per genotype, 20 sections per animal. **c**, E17.5 *Mfsd2a*$^{-/-}$ mice exhibit normal pericyte–endothelial attachment. High magnification images of capillary cross sections co-staining for endothelium (Glut1, red) and pericytes (Pdgfrβ, green) revealed no difference in pericyte-endothelial relationships between wild-type (top panels) and *Mfsd2a*$^{-/-}$ (bottom panels) mice (endothelial nucleus and pericyte nucleus are indicated by single and double asterisks, respectively). **d**, Electron micrographs of longitudinal capillary sections revealed that pericytes had normal appearance and were well positioned on the vessel walls in *Mfsd2a*$^{-/-}$ adult mice; pericytes were adjacent to endothelial cells and shared a common basement membrane. L, lumen; P, pericyte.

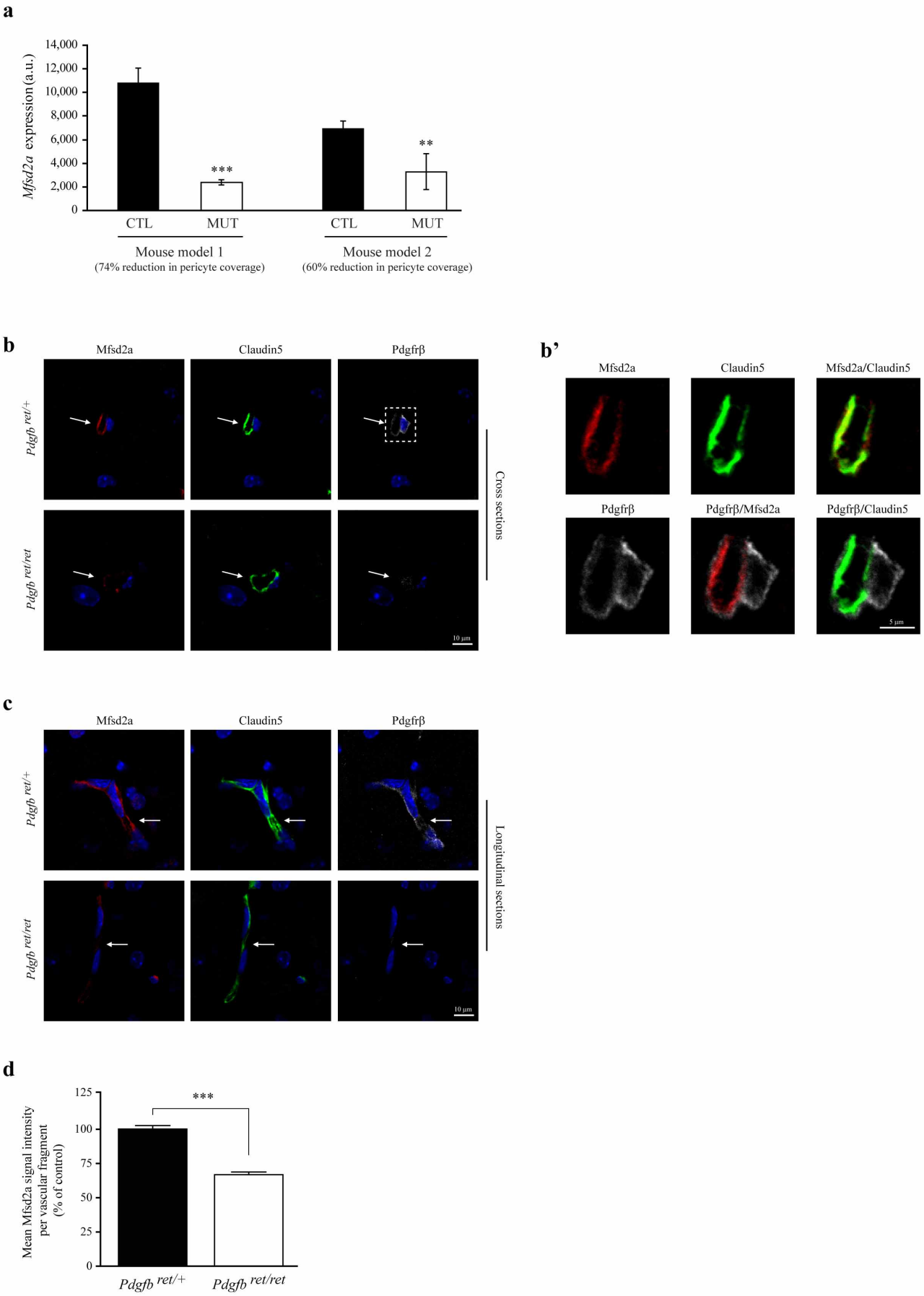

Extended Data Figure 7 | *Mfsd2a* gene expression and Mfsd2a protein levels are downregulated in mouse models of reduced pericyte coverage. **a**, Analysis of microarray data[5] showed high levels of *Mfsd2a* expression in wild-type adult brain microvasculature, but a significant decrease in levels of *Mfsd2a* expression in mice that have reduced pericyte coverage at the BBB. $Pdgfb^{ret/ret}$ mice (mouse model 1), where Pdgfβ binding to heparan sulphate proteoglycans was disrupted, exhibited a major loss of pericyte coverage (74% reduction)[5] and showed a dramatic decrease in *Mfsd2a* expression (74% reduction) compared to that of littermate controls. Similarly, $Tie2^{Cre}/R26^{P+/0}$, $Pdgfb^{-/-}$ mice (mouse model 2) in which *Pdgfb*-null alleles were complemented by one copy of human *PDGFB* transgene showed a less dramatic loss of pericyte coverage (60% reduction)[5] and a smaller decrease in *Mfsd2a* expression (53% reduction). $^{**}P = 0.004$, $^{***}P = 1 \times 10^{-5}$). Bars reflect normalized signal of the *Mfsd2a* probe (1428223_at) in adult brain or cortex microvascular fragments (a.u.). Data are mean ± s.d. of 4 biological replicates. **b**, Mfsd2a immunostaining in cerebrovasculature of postnatal $Pdgfb^{ret/ret}$ mice and littermate controls ($Pdgfb^{ret/+}$) revealed reduced Mfsd2a protein expression in endothelial cells that are not covered by pericytes. Cross section: red, Mfsd2a; green, claudin-5 (endothelium); blue, DAPI (nuclei); grey, Pdgfrβ (pericyte). Reduced Mfsd2a signal was observed in endothelial cells of capillaries not covered with pericytes in $Pdgfb^{ret/ret}$ mice (arrow, bottom panels), whereas strong Mfsd2a signal was apparent in pericyte-covered capillaries in $Pdgfb^{ret/+}$ mice (arrow, top panel). Insets in **b′** demonstrate in high magnification that Mfsd2a expression is restricted to endothelial cells (co-localization with claudin-5 staining) and absent in pericytes (none co-localization with Pdgfrβ staining). **c**, Additional example of the reduction in Mfsd2a expression in endothelial cells of $Pdgfb^{ret/ret}$ mice (longitudinal section). **d**, Quantification of mean fluorescence intensity per vascular profile showed significant reduction of Mfsd2a signal in $Pdgfb^{ret/ret}$ capillaries compared to controls. Data are mean ± s.e.m. $n = 2$ animals per genotype, 60 images quantified of at least 600 vascular profiles per animal.

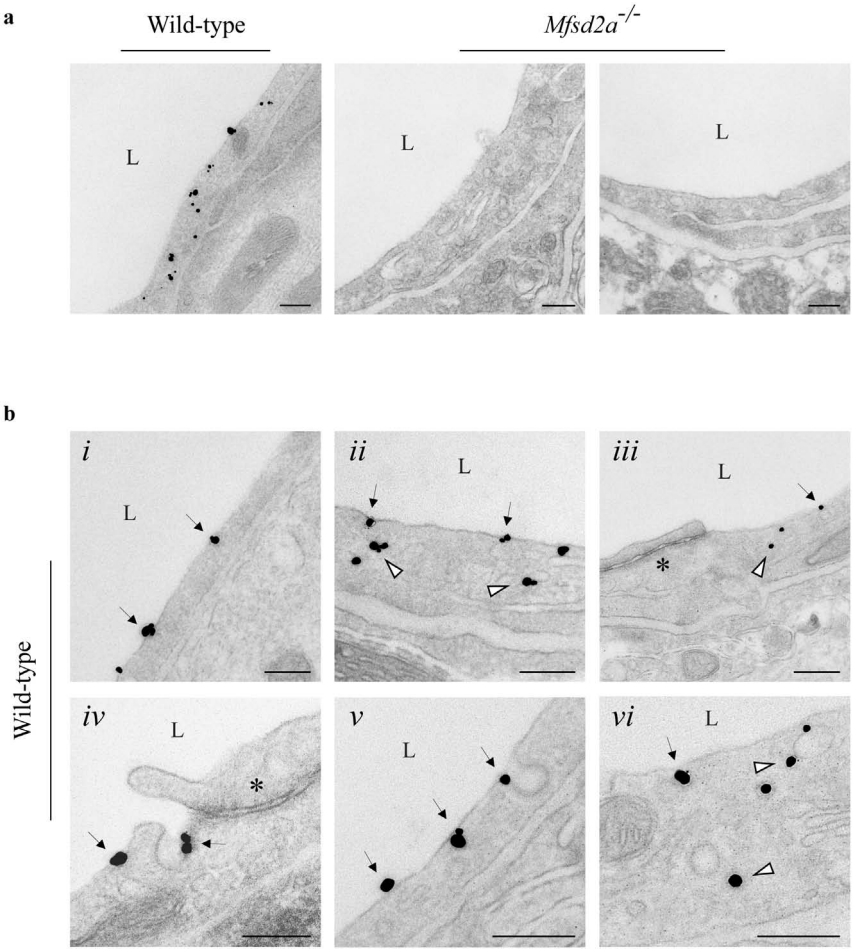

Extended Data Figure 8 | Immuno-electron-microscopy reveals the subcellular localization of Mfsd2a on the plasma membrane and vesicles, but not in tight junctions of cerebral endothelial cells. **a**, Electron micrographs showing silver-enhanced immunogold labelling of Mfsd2a in cerebral cortex capillaries from wild-type (left) but not in *Mfsd2a*$^{-/-}$ mice (right), demonstrating staining specificity. **b**, Top panels (*i–iii*), three representative examples of Mfsd2a localization on the plasma membrane (arrows) and in the cytoplasm (arrowheads), but not in tight junctions (asterisk). Bottom panels (*iv–vi*), high magnification representative examples of Mfsd2a localization on the luminal plasma membrane (arrows), associated with luminal invaginating vesicles (*iv, v*) and with cytoplasmic vesicles (arrowheads). All samples are of cortical vessels from adult mice (P30–P90). $n = 2$ for each genotype. L, lumen.

Extended Data Table 1 | Expression-profile comparison of cortex (BBB) and lung (non-BBB) endothelial cells

a

Probe set	Gene Symbol	Cortex GFP+	Lung GFP+	Cortex/Lung
1418788_at	Tie2	2765.0	5040.7	0.5
1417839_at	Cldn5	4978.0	4709.7	1.1
1440926_at	flt1	771.5	606.1	1.3
1449379_at	VegfR2	3578.6	2115.3	1.7
1433956_at	VE-cadherin	2422.9	3572.4	0.7
1421287_a_at	PECAM	364.4	725.4	0.5

b

Probe set	Gene Symbol	Cortex GFP+	Lung GFP+	Cortex/Lung
1423343_at	Slco1c1	2918.1	51.7	56.4
1454622_at	Slc38a5	3007.5	124.7	24.1
1435418_at	Slc22a8	253.6	11.28	22.5
1448299_at	Slc1a1	565.9	47.4	11.9
1418706_at	Slc38a3	917.2	117.9	7.8
1418326_at	Slc7a5	5913.1	1050.9	5.6
1433933_s_at	Slco2b1	994.3	207	4.8
1447227_at	Slc40a1	81.8	20.3	4.0
1436137_at	Slc6a17	567	147.5	3.8
1436417_at	Slc19a3	124.6	34.4	3.6
1451486_at	Slc46a3	371.3	112.2	3.3
1422906_at	Abcg2	458.6	166.2	2.8
1436164_at	Slc30a1	2768	1178.4	2.3
1434773_a_at	Slc2a1	9337.6	4144.4	2.3
1419759_at	Abcb1a	1520	676.8	2.2
1454991_at	Slc7a1	8403.4	4403.5	1.9
1429154_at	Slc35f2	369.6	211	1.8
1433751_at	Slc39a10	3222.8	2074.3	1.6
1437149_at	Slc6a6	2096.5	1367.6	1.5
1433750_at	Slc31a1	1666.4	1389.2	1.2
1447851_x_at	Atp10a	328.4	276.6	1.2
1443870_at	Abcc4	138.4	117.5	1.2
1424211_at	Slc25a33	99.2	93	1.1
1426082_a_at	Slc16a4	94.3	95.8	1.0
1418445_at	Slc16a2	1953.4	2069.4	0.9
1415802_at	Slc16a1	925.1	989.5	0.9
1423109_s_at	Slc25a20	310.4	410.7	0.8
1417022_at	Slc7a3	51.5	74.4	0.7
1453149_at	Slc25a32	109.2	204.7	0.5

a, Pan-endothelial markers were highly expressed in endothelial cells isolated from both cortex and lung of the endothelial specific *Tie2-GFP* reporter mouse at E13.5. **b**, Genes involved in the transport of molecules across the BBB, known as adult BBB markers, were highly enriched in brain versus lung endothelial cells. Data are mean of 4 biological replicates (4 litters).

Extended Data Table 2 | Vesicular activity and transcytosis events in the brain endothelial cells of *Mfsd2a*$^{-/-}$ mice are dramatically increased

a

Density of vesicles in the embryo brain endothelium (E17.5)

Tissue source	No. of endothelial profiles	No. of vesicles	Mean vesicular density			
			Luminal type I vesicles (/μm)	Luminal type II vesicles (/μm)	Cytoplasmic vesicles (/μm²)	Abluminal vesicles (/μm)
Controls	40	1180	0.34 ± 0.05	0.14 ± 0.03	2.04 ± 0.06	0.21 ± 0.03
Mfsd2a$^{-/-}$	40	2449	0.62 ± 0.03 **	0.38 ± 0.03 ***	4.62 ± 0.30 ***	0.48 ± 0.04 ***

b

Density of HRP-filled vesicles in adult brain endothelium (P90)

Tissue source	No. of endothelial profiles	No. of HRP-filled vesicles	Cytoplasmic HRP^{+} vesicles (/μm²)
Controls	15	0	0
Mfsd2a$^{-/-}$	15	97	3.35 ± 0.55

a, Quantification of the vesicular density (both total and individual type of vesicles) in E17.5 control and mutant endothelium. Mean vesiclar density was calculated from the number of vesiclar types per μm of luminal membrane (luminal type I and type II vesicles), per μm^2 of cytoplasm (cytoplasmic vesicles), and per μm of abluminal membrane (abluminal vesicles). **b**, Quantification of HRP luminal uptake in P90 HRP-injected mice. No HRP-filled vesicles were found in wild-type mice. Data are mean ± s.e.m. from 4 controls and 4 mutants (10 vessels per animal, 2 images at ×12,000 per vessel). $^{**}P < 0.01$, $^{***}P < 0.001$, using Student's *t*-test.